### nature communications



**Article** 

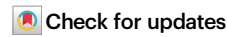
https://doi.org/10.1038/s41467-025-65438-z

# Bennu and Ryugu constituents from samples IR analyses and potential source of terrestrial planets' ingredients

Received: 25 May 2025

Accepted: 13 October 2025

Published online: 04 November 2025



C. Pilorget  $f 0^{1,2} \boxtimes$ , T. Okada  $f 0^{3,4}$ , J.-P. Bibring 1, D. Loizeau 1, K. Hatakeda 3,5,

L. Nardelli 1, L. Riu<sup>6</sup>, R. Sheppard<sup>1,7</sup>, T. Jiang<sup>1,8</sup>, M. Mahlke<sup>1,9</sup>, R. Brunetto 1,

D. Baklouti 1, R. Fukai, M. Abe, A. Aléon-Toppani, Y. Enokido, V. Hamm,

S. Kawasaki<sup>3</sup>, C. Lantz 1, A. Miyazaki<sup>3</sup>, A. Moussi-Soffys<sup>10</sup>, M. Nishimura 1, A. Moussi-Soffys<sup>10</sup>, M. Nishimura 1, A. Miyazaki<sup>3</sup>, A. Miyazak<sup>3</sup>, A. Miyazak<sup>3</sup>, A. Miyazak<sup>3</sup>, A. Miyazak<sup>3</sup>, A. Miyazak<sup>3</sup>, A. Miya

F. Poulet<sup>1</sup>, R. Tahara<sup>3</sup>, T. Usui D<sup>3,4</sup>, T. Yada D<sup>3</sup> & K. Yogata D<sup>3</sup>

Samples collected on carbonaceous asteroids and preserved from terrestrial alteration are key witnesses of the early evolution of the Solar System. Here we present the results of the characterization, by the near-IR hyperspectral microscope MicrOmega within the ISAS/JAXA curation center, of the samples returned from the Bennu asteroid by the OSIRIS-REx mission. We compare these samples to those from Ryugu, analyzed with the same instrument and at the same facility, using gram-scale quantities of material. We demonstrate that Bennu and Ryugu samples exhibit similar near-IR diagnostic spectral properties, from the centimetre down to the sub-millimetre scale. A wide variety of compounds are detected within a similar phyllosilicate-rich matrix, including diverse carbonates, H<sub>2</sub>O-rich and NH-rich phases, and notably Hydrated Ammonium-Magnesium-Phosphorus-rich grains. Rarely, anhydrous silicates are also observed. Despite some minor, although significant differences, our results indicate that the parent bodies of Ryugu and Bennu share similar formation and early evolution processes in the outer protoplanetary disk. Their main characteristics would, thus, define an entire class of objects which might have driven specific evolutionary pathways for terrestrial planets, including that which led to life on Earth.

Carbonaceous asteroids record processes that occurred during the early evolution of the Solar System. They may have also critically contributed to the delivery of chemical compounds to the terrestrial planets (e.g.¹,). Samples from these objects have been collected and successfully returned to Earth, first by the JAXA Hayabusa2 mission from the C-type asteroid Ryugu in December 2020², and more recently in September 2023 by the NASA OSIRIS-REx mission from the B-type

asteroid Bennu<sup>3</sup>. For the first time, these collections offer a unique access to material directly collected on carbonaceous asteroids, presumed free from terrestrial contamination and alteration, contrary to meteorites.

Analyses of Ryugu samples have shown that their elemental, isotopic and mineralogical composition are most similar to CI-type chondrites (e.g., <sup>2,4-12</sup>). As such, Ryugu mineralogical composition

<sup>1</sup>Institut d'Astrophysique Spatiale, Université Paris-Saclay, CNRS, Orsay, France. <sup>2</sup>Institut Universitaire de France, Paris, France. <sup>3</sup>Institute of Space and Astronautical Science, Japan Aerospace Exploration Agency, Sagamihara, Japan. <sup>4</sup>Graduate School of Science, University of Tokyo, Tokyo, Japan. <sup>5</sup>Marine Works Japan, Ltd., Yokosuka, Japan. <sup>6</sup>ESAC, Camino Bajo del Castillo s/n, Madrid, Spain. <sup>7</sup>Planetary Science Institute, Tucson, AZ, USA. <sup>8</sup>Muséum National d'Histoire Naturelle, Paris, France. <sup>9</sup>Institut UTINAM, Observatoire de Besançon, Besançon, France. <sup>10</sup>Centre National d'Etudes Spatiales, Toulouse, France. <sup>2</sup>Me-mail: cedric.pilorget@universite-paris-saclay.fr

consists principally of phyllosilicates (serpentine- and saponite-type), carbonates, sulfides, magnetite and phosphates (e.g., <sup>5,7,8</sup>). Various CHNOS-based organic materials and rare anhydrous silicates (olivine and pyroxene) have also been reported (e.g., <sup>8,9,13,14</sup>). However, major differences could be observed between Ryugu samples and CI chondrites. In particular Ryugu samples are much darker than CI chondrites with reflectance as low as 2-3 % (e.g., <sup>2,4,8</sup>) (vs 4-5% for CI chondrites). Analyses of the Ryugu samples have also highlighted the presence of Hydrated Ammonium-Magnesium-Phosphorus (HAMP)-rich compounds<sup>15</sup>, that were as of yet not observed in meteorites. Some others compounds such as sulfates and ferrihydrite were, however, absent (e.g., <sup>5</sup>), as well as most of the interlayer water in the phyllosilicates<sup>7,12</sup>.

While some of the differences may reflect variations in the initial conditions (e.g., composition, formation environment) or the subsequent evolution of the parent bodies, exposure of asteroid material to the terrestrial atmosphere has been shown to significantly alter both its mineralogical properties<sup>16,17</sup> and its water budget<sup>7,12,18</sup>. These results strongly support maintaining returned carbonaceous asteroids samples in pristine conditions, meaning free from terrestrial alteration and thus preserving their properties at collection, for at least initial characterization.

First results obtained from the Bennu samples have also shown some similarities with CI chondrites regarding elemental and mineralogical composition3. In particular, Mg-rich phyllosilicates (primarily serpentine and smectite), magnetite, sulfides, carbonates and phosphates have been identified in the bulk samples<sup>3,19</sup>. However, some differences were also observed from the Ryugu samples. Carbon and nitrogen abundances were found to be significantly higher in Bennu samples<sup>3,14</sup>. H and N isotopic analyses on Bennu samples have also shown some small but significant differences from CI chondrites and Ryugu material. While Ryugu's  $\delta^{15}N$  and  $\delta D$  compositions  $(\delta^{15}N = 43.0 \pm 9.0\%, \delta D = 252 \pm 13\%^{14})$  are consistent with those of CI chondrites, Bennu's  $\delta^{15}N$  and  $\delta D$  compositions ( $\delta^{15}N = 82 \pm 15\%$ ,  $\delta D = 344 \pm 13\%$ . are closer to those of the Tarda and Tagish Lake meteorites (C2-ungrouped), raising the question of the potential connection that exists between their parent bodies and the processes that drove their evolution.

Through an agreement between NASA and JAXA, samples from Ryugu and Bennu were exchanged between the two agencies. As a result, -0.6 g of Bennu samples were extracted from the collection as

five different bulk samples and delivered in August 2024 to the Extraterrestrial Sample Curation Center of JAXA (ESCuC, Sagamihara, Japan)<sup>20</sup>. Similarly to Ryugu samples, pristine Bennu samples (never exposed to the terrestrial environment) are stored in a pure  $N_2$ -purged controlled chamber. There they are submitted to a first round of preliminary examination with a suite of instruments including the near-IR hyperspectral microscope MicrOmega<sup>21</sup>. This instrument was already used for the characterization of the Ryugu sample collection<sup>4,II,12,I5,18,22</sup>, enabling a direct comparison and unique crossanalysis between both collections of samples.

We present here an assessment of the IR spectral diversity observed in Bennu samples, while in their pristine state, and a first comparison with Ryugu samples.

#### **Results**

#### Centimetre to millimetre spatial scale

At the scale of a few mm, MicrOmega analyses of the five Bennu bulk samples delivered to JAXA reveal that they are dominated by a dark matrix (-2–3% reflectance at 2.5  $\mu m)$  with a red slope at shorter wavelengths, a ~ 2.72  $\mu m$  absorption consistent with OH moieties (O–H stretching) strongly bonded to Mg (most likely in Mg-rich phyllosilicates) and a weaker ~3.4  $\mu m$  feature attributable to the presence of organic compounds and/or carbonates (Fig. 1 a, Supplementary Fig. 1), consistent with²0.

The ~2.7 µm absorption band exhibits an asymmetric shape with a more pronounced right wing. Importantly, there is no significant contribution of the O-H stretching mode of H<sub>2</sub>O molecules around 3 µm. All Bennu bulks show a similar 2.7 µm band profile (Fig. 1b, Supplementary Fig. 2). The peak position is estimated at  $2.717 \pm 0.005 \,\mu m$  and the relative band depth varies in the 10-12% range (Supplementary Fig. 2). Some slight variability is, however, observed in the band position (with typical shifts <10 nm to longer wavelengths), depth or shape (with slightly more pronounced right wings) in some mm-sized grains (Fig. 1b, c). The relative band depth of the ~3.4 µm feature typically varies in the 3-4% range (Fig. 1a. Supplementary Fig. 1). Its shape, more pronounced at ~3.42 µm, indicates that the signature of organics (aliphatic CH, e.g., ), dominates over that of carbonates (which would show a doublet at ~3.3–3.5 µm) when integrating over areas a few mm wide. These organic compounds are presumably mixed with other matrix constituents at sub-micron scale, but local enrichments at larger scale could also be present, as within the Ryugu samples<sup>4</sup>.

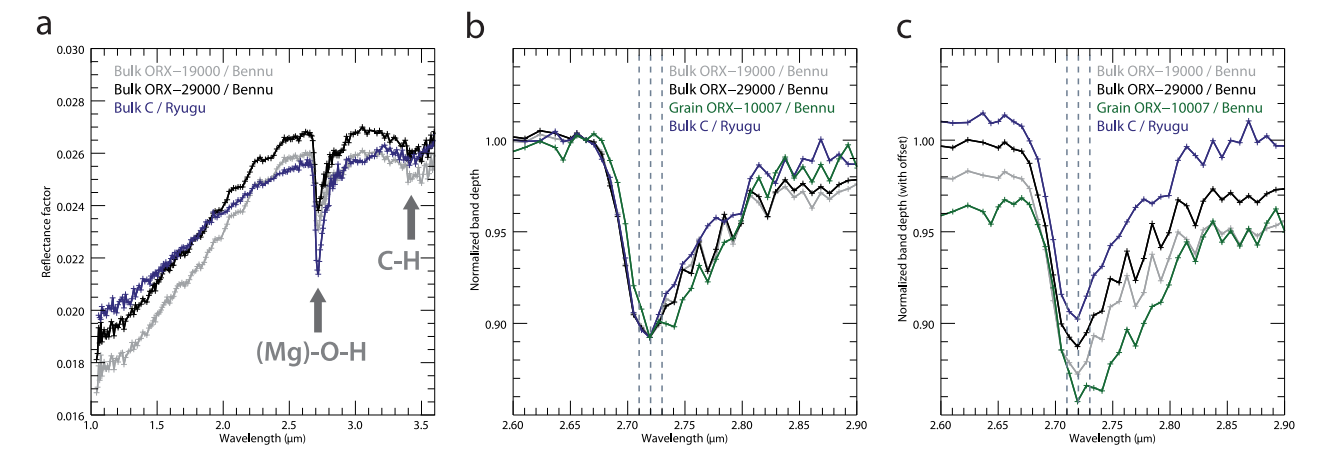


**Fig. 1** | **IR spectral characterization of bulk samples. a** Typical MicrOmega spectra at the scale of a few mm within Bennu bulks ORX-19000 and ORX-29000, compared to Ryugu bulk spectrum from chamber  $C^4$ . **b** Normalized 2.7  $\mu$ m absorption band. The average spectrum of mm-size grain ORX-10007 (extracted from bulk ORX-19000, Bennu) has been added for comparison. Both the band

depth and the continuum were normalized to that of ORX-29000 spectrum to enable a comparison of the band shapes and positions. Vertical dashed lines are set at 2.71, 2.72 and 2.73  $\mu m$  to highlight differences in peak positions. **c** Same as (**b**) with offset for clarity.

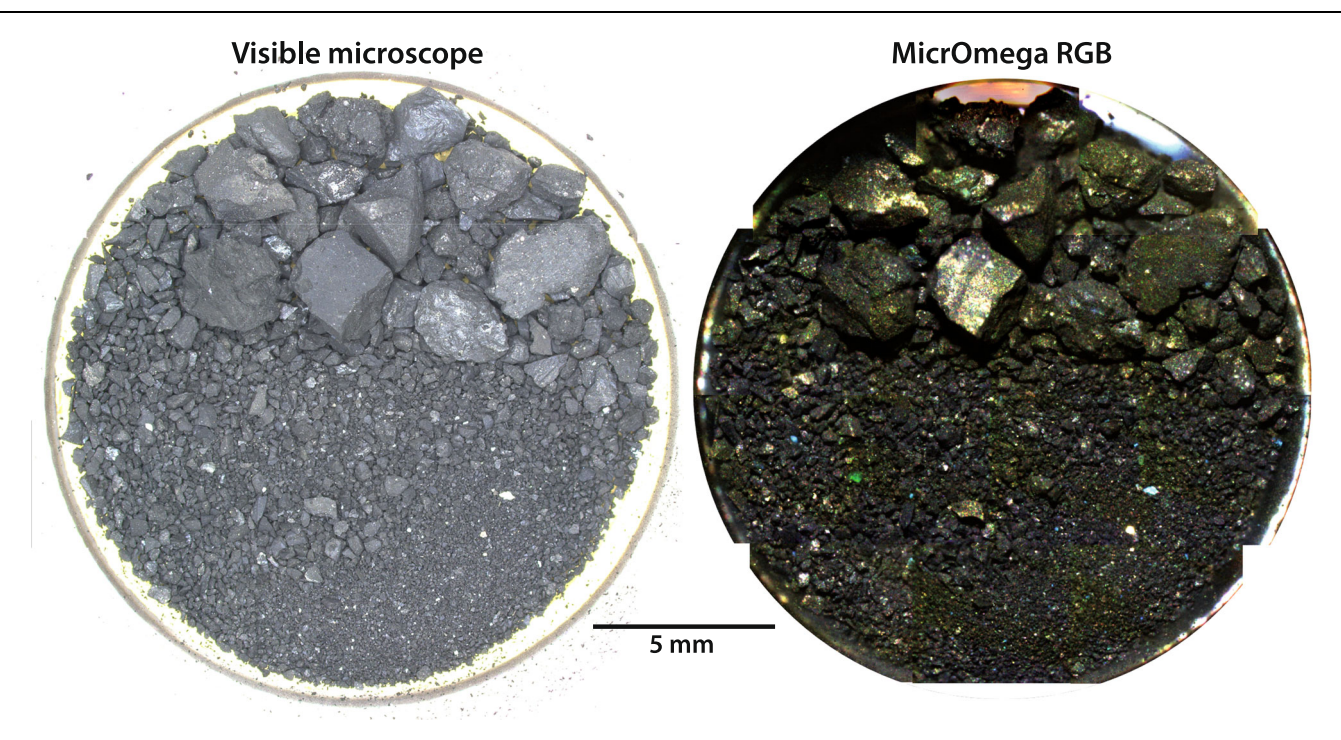


Fig. 2 | Visible and IR images of bulk samples. Bulk ORX-29000 observed by the Leica visible microscope and by the MicrOmega IR hyperspectral microscope (Mosaic of RGB composite images). The following wavelengths are used for the MicrOmega RGB image: R: 3.34 μm, G: 2.50 μm, B: 1.20 μm.

#### Sub-millimetre spatial scale

At sub-mm scale, we identified within the dark matrix a great variety of grains and inclusions larger than a few tens of micrometres (Micromega spatial sampling is  $22.5 \times 22.5 \,\mu\text{m}^2$ ) with different spectral signatures. Most of them have a much higher reflectance factor (-5–20%) than the matrix. We can typically observe a few tens of them at the surface of each bulk sample (Fig. 2).

The first family of spectra that are commonly found (Type 1) exhibits a ~ 3.3-3.5 µm absorption feature diagnostic of carbonates (combination modes and overtones of the fundamental stretching and bending modes in CO<sub>3</sub>) (Fig. 3). These spectra are associated with bright grains and inclusions (reflectance factor of ~5-15%) ranging in size from a few tens to a few hundred of micrometres. They appear variously as clusters of small inclusions (tens of micrometres in size) on grains dominated by the phyllosilicate-rich matrix, as long vein-like features, or as more diffuse distributions throughout the grain. Additional ~2.3 µm, ~2.5 µm and ~2.8 µm features are also sometimes observed in the largest detections. These weaker features are associated with combination modes of carbonates  $(3v_3, v_1 + 2v_3)$  and  $2v_3 + v_4$ , respectively, with  $v_1$  the symmetric CO<sub>3</sub> stretching mode,  $v_3$ the asymmetric stretching and v<sub>4</sub> the in plane-bending). A strong red slope below 1.5 µm can also be observed for a fraction of the carbonates, attesting to the presence of Fe<sup>2+</sup> among the cations. Notably, a ~ 2.7 µm feature is also present. The position and shape of the ~3.3-3.5  $\mu$ m feature are indicative of the main cations coupled to  $CO_3^{2}$  (e.g., <sup>23,24</sup>). Following the methods developed by refs. 11 and <sup>25</sup>, we were able to identify at least two families of significant importance: dolomite (CaMg(CO<sub>3</sub>)<sub>2</sub>) and breunnerite ((Mg,Fe)CO<sub>3</sub>) (Fig. 3). Such carbonates have also been identified by complementary methods by refs. 3,17,19. Both types of carbonates exhibit spectra very similar to those of the Ryugu samples, in particular the presence of a 2.7 µm feature, which may reflect small-scale mixing of matrix material with the carbonates<sup>11</sup>.

A second common family of spectra (Type 2) exhibits a deep and broad -3  $\mu$ m absorption feature that we attribute to the O-H stretching mode of H<sub>2</sub>O molecules (e.g., <sup>26</sup>). In most cases, either a sharp peak or a shoulder at -2.7  $\mu$ m can be observed on the left edge of the band (Fig. 4i

- spectra A,B,C,D). Weak absorptions between ~3.0 and 3.3 μm are also sometimes present. Such spectral features are generally associated with bright, detached grains (reflectance factor of ~10-20%), but inclusions in millimetre-sized matrix-dominated grains have also been observed. Grain sizes range from a few tens to a few hundreds of micrometres. Many detached grains exhibit a whitish, uniform appearance in optical images, punctuated by smaller, dark micrometre-sized grains that seem either embedded within the whitish material or stuck to the surface (Fig. 4a). These smaller grains may be leftovers from the surrounding matrix when the bright grain was detached, but we cannot rule out the presence of deeper inclusions. Other detached grains might appear as clusters of smaller bright units and dark material. The bright inclusions found in millimetre-sized grains and that exhibit a deep and broad ~3 µm absorption have various complex morphologies, sometimes as veins running through the grain (Fig. 4d), and sometimes as aggregates of bright inclusions a few tens to a few hundreds of micrometres in size (Fig. 4b). Notably, they tend to have a whitish to whitish-bluish appearance in the optical images, suggesting some variability in their composition. Complementary mid-IR spectra obtained with a μ-FT-IR spectrometer (see Methods) on inclusions/grains displaying such a signature exhibit a ~ 6.1 µm as well as a ~ 6.9 µm absorption band that we attribute respectively to the presence of H<sub>2</sub>O (bending mode v<sub>2</sub>, e.g., <sup>27,28</sup>), and NH<sub>4</sub><sup>+</sup> (out of plane bending mode  $v_4$ , e.g.,  $^{29,30}$ ). In particular, the presence of  $NH_4^+$  could explain the spectral bands observed between 3.0 and 3.3 µm in MicrOmega data (e.g., 30). Additionally, a broad feature between ~9 μm and 10 µm attributed to P-O stretching vibrations (e.g., 31,32) can also be observed. Similar spectral signatures have also been observed in Ryugu samples<sup>15</sup>, indicating the presence of Hydrated Ammonium-Magnesium-Phosphorus (HAMP)-rich compounds. The specific and diagnostic ~3 µm (on pristine samples), ~6.9 and ~9.5 µm band shape, position, and depth are similar between Ryugu and Bennu HAMP-rich compounds.

A third family of spectra (Type 3) – quite rare (about a dozen of occurrences in the bulk samples) - exhibits both -2.7  $\mu$ m and -3.05  $\mu$ m features (Fig. 5). The -3.05  $\mu$ m band is attributed to the N-H stretching vibration (e.g., 30), in NH<sub>4</sub><sup>+</sup> or in NH-rich organics for instance. The

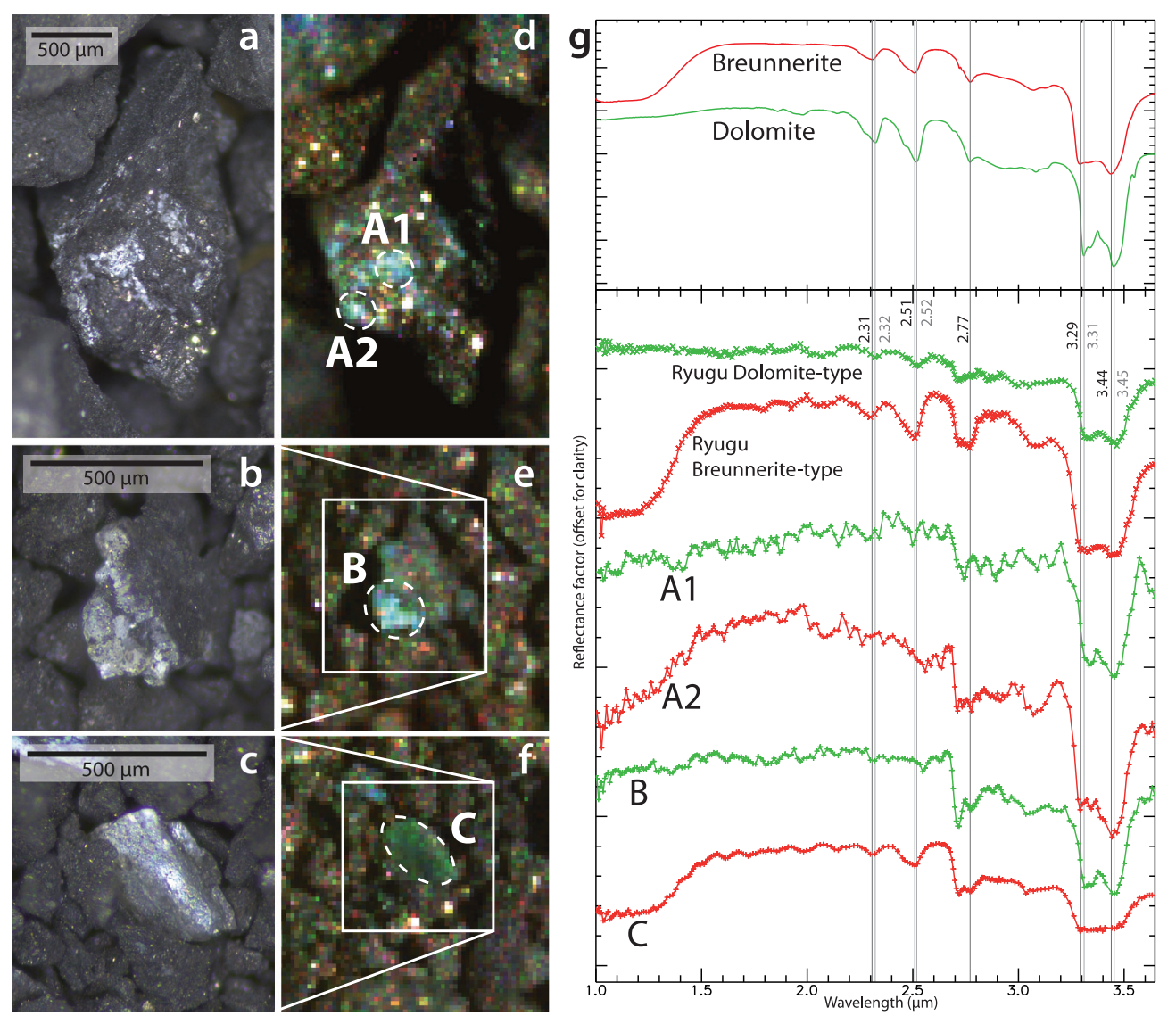


Fig. 3 | Examples of Type 1 spectra (carbonates) observed by MicrOmega within Bennu bulk samples. a-c Visible images show the context where these carbonate inclusions are detected. In MicrOmega RGB composite images of the same areas (d-f), carbonates appear in shades of green and blue (R: 3.34 μm, G: 2.50 μm, B: 1.20 μm). g Average MicrOmega spectra of the carbonate-rich regions highlighted by the dashed circles on the MicrOmega RGB images (Al averages 19 pixels, A2: 10

pixels, B: 50 pixels, C: 89 pixels). Examples of carbonates identified in Ryugu pristine samples by MicrOmega under similar conditions<sup>11</sup> are shown for comparison. Reference spectra of terrestrial carbonates are also displayed (dolomite BKR1CB017a spectrum from RELAB and a terrestrial breunnerite spectrum acquired at IAS, Orsay<sup>11</sup>).

 $2.72\,\mu m$  feature is attributed to the stretching vibration of O-H strongly bonded to Mg atoms that we typically find in Mg-rich phyllosilicates (e.g., <sup>33</sup>). Together, these indicate an NH-bearing species associated with a MgOH-rich material, plausibly a phyllosilicate similar to that of the matrix, as shown by the shape and position of the band. A weak -2.32  $\mu m$  feature can also sometimes be observed which we attribute to combination vibrations involving the O-H stretch and the bend of O-H strongly bonded to Mg atoms (e.g., <sup>34</sup>). Its presence is fully consistent with that of the  $2.72\,\mu m$  feature, in particular in the context of high albedo which increases the visibility of spectral features compared to dark material. This spectral family is generally associated with bright whitish to yellowish inclusions (reflectance factor of ~5–20% typically), with sizes from a few tens to a few hundreds of micrometres (Fig. 5a). The spectral properties of these inclusions closely resemble those observed in Ryugu samples.

A fourth kind of spectral family (Type 4a) – very rare (only a few occurrences) - exhibits a strong <1.6  $\mu$ m slope and a flat continuum at

longer wavelengths which is consistent with olivine (Fig. 6e - spectrum A). This signature was observed for several ~50-100  $\mu m$  large, detached bright grains (reflectance factor of ~5–10 %). Complementary mid-IR spectral data were also obtained for one such grain. It shows a broad feature at ~10  $\mu m$  with 3 distinct sub-features at ~9.8, ~10.3 and ~10.8  $\mu m$ , confirming the olivine attribution (Fig. 6e – spectrum A). Additional features between ~4.8 and 6  $\mu m$  are also interpreted as Si-O combination and overtone modes of crystalline olivine (e.g.,  $^{35,36}$ ). The position of the 3 sub-features around 10  $\mu m$  in this grain is indicative of Mg/(Fe+Mg)#~60%  $^{37-39}$ . Such specific composition might, however, not be representative of all the olivine detections. In addition, a small feature at ~2.7  $\mu m$  due to OH moieties strongly bonded to Mg atoms can be noticed in the mid-IR spectrum. As the grain size is close to the observation spot size, such a signature most likely originates from the neighboring grains.

In one particular case (Type 4b), we observe both a strong  $<1.6\,\mu m$  slope and a broad asymmetrical  $3\,\mu m$  feature with an

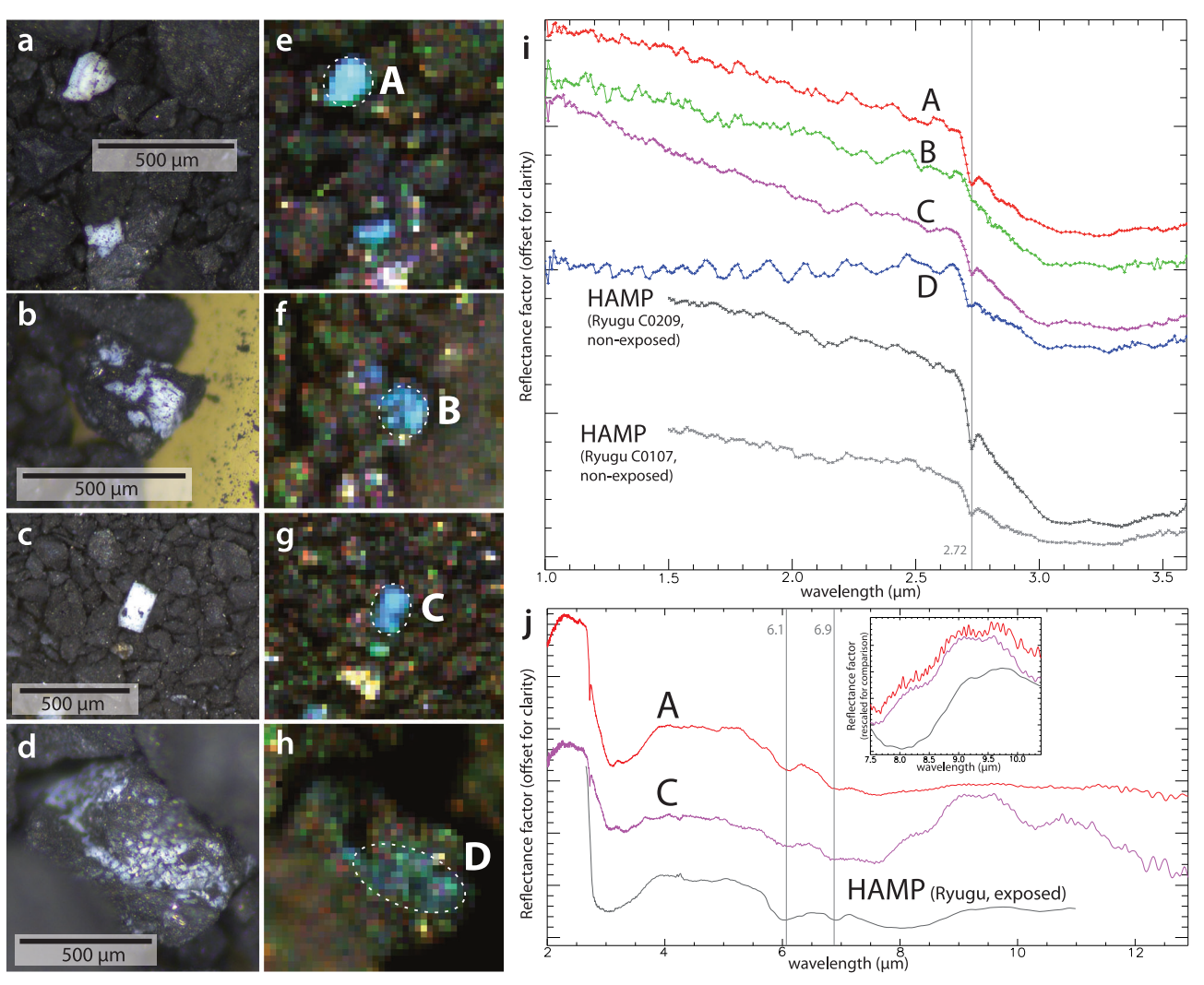


**Fig. 4** | **Examples of Type 2 spectra (hydration feature at 3 μm) observed by MicrOmega within Bennu bulk samples.** a–d Visible images show the context where these inclusions/grains are detected. In MicrOmega RGB composite images of the same areas (**e**–**h**), they appear in shades of green and blue (R: 3.34 μm, G: 2.50 μm, B: 1.20 μm). **i** Average MicrOmega spectra of the regions highlighted by the dashed circles on the MicrOmega RGB images (region A: 31 pixels, region B: 28 pixels, region C: 60 pixels, region D: 63 pixels). HAMP spectra, measured in Ryugu samples by the same MicrOmega instrument while the samples were kept pristine in their preservation chamber are shown for comparison<sup>15</sup>. **j** Complementary mid-IR spectral data obtained on Areas A and C with a μ-FT-IR spectrometer. These

combined near-IR-mid-IR analyses did not require any extraction from the facility, preventing any exposure of the sample to the terrestrial environment. A HAMP spectrum, measured ex-situ in Ryugu samples by a  $\mu\text{-FT-IR}$  instrument, is shown for comparison  $^{15}$ . The latter displays a slightly broader 3  $\mu\text{m}$  band due to absorption/adsorption of atmospheric water. An insert with rescaled reflectance factor provides a better view at the -9.5  $\mu\text{m}$  feature attributed to the P-O stretching vibration. Indeed, the intensity of this feature is quite sensitive to local geometric conditions and might significantly vary between the samples. The weak features between 3.3 and 3.6  $\mu\text{m}$  in spectrum B are artifacts.

additional and prominent component at ~2.8 µm compared to Type 2 spectra (Fig. 6e - spectrum B). A small feature at ~3.5 µm can also be observed. This signature has been detected in a whitish-yellowish inclusion about 300 µm in size with a complex morphology (Fig. 6b). A complementary mid-IR spectrum of the inclusion exhibits two sharp peaks at ~9.5 and ~10.6 µm, as well as a smaller feature at ~10.3 µm. Possible small absorption bands between ~4.8 and ~6 µm are also observed. The combination of the <1.6 µm slope, the features between ~9.5 and ~10.6 µm and that between ~4.8 and ~6 µm are consistent with olivine (though with a smaller ~10.3 µm feature compared to the two main peaks). The additional presence of a ~ 3  $\mu$ m absorption band, due to the O-H stretching mode of H<sub>2</sub>O, is quite surprising. The explanation can come from the ~2.8 µm absorption feature which can be due to the SiO-H vibration (e. $g_{*}^{40,41}$ ,). This would then indicate that this olivine, in which  $H_2O$  is present, probably as ad/absorbed molecules, is hydroxylated, i.e. slightly altered compared to that shown in spectrum A of Fig. 6e.

The position of the main peaks at -9.5 and -10.6 μm, would also point toward a composition richer in Mg (Mg/(Mg+Fe)#-70%).

#### Discussion

At the scale of a few millimetres, the Bennu samples analyzed in this work exhibit spectral properties in the near-IR range that are similar to the ones of Ryugu pristine samples: a reflectance factor of 2-3 % at 2.5  $\mu$ m, a red slope from -1.0 to 2.5  $\mu$ m and two main absorption bands at -2.7  $\mu$ m and -3.4  $\mu$ m<sup>4</sup>. The absence of a significant -3  $\mu$ m contribution to the matrix spectra, similar to the one observed in the spectra of CI chondrites and air exposed Ryugu samples (e.g. <sup>12,18,33</sup>,), confirms that the samples have never been exposed to the terrestrial environment since their collection from the asteroid (i.e. pristine). This also indicates that the phyllosilicates, notably the smectites, are comparatively poor in interlayer water molecules. The position of the -2.7  $\mu$ m, at 2.717  $\pm$  0.005  $\mu$ m, is consistent with the presence of Mg-rich phyllosilicates (e.g., <sup>33,42</sup>). The -2.7  $\mu$ m band is also similar to the one observed

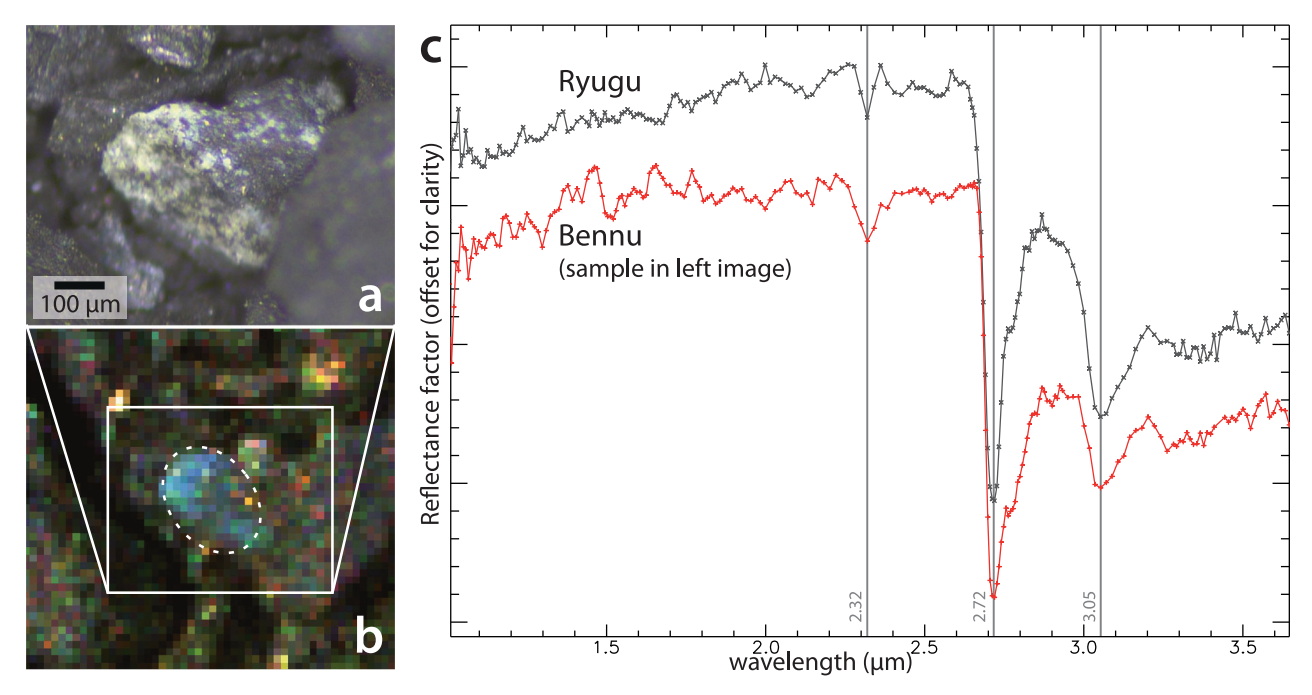


Fig. 5 | Example of a Type 3 spectrum (NH-/MgOH-rich inclusion) observed by MicrOmega within Bennu samples. a Visible image shows the context where the inclusion is detected. In MicrOmega RGB composite image of the same area (b), it appears in shades of blue (R:  $3.34 \mu m$ , G:  $2.50 \mu m$ , B:  $1.20 \mu m$ ). c MicrOmega average

spectrum indicated by the dashed circle (120 pixels). A 'Type 3' spectrum measured in Ryugu samples by the same MicrOmega instrument in similar conditions is shown for comparison (from Ryugu Bulk C<sup>4,44</sup>,).

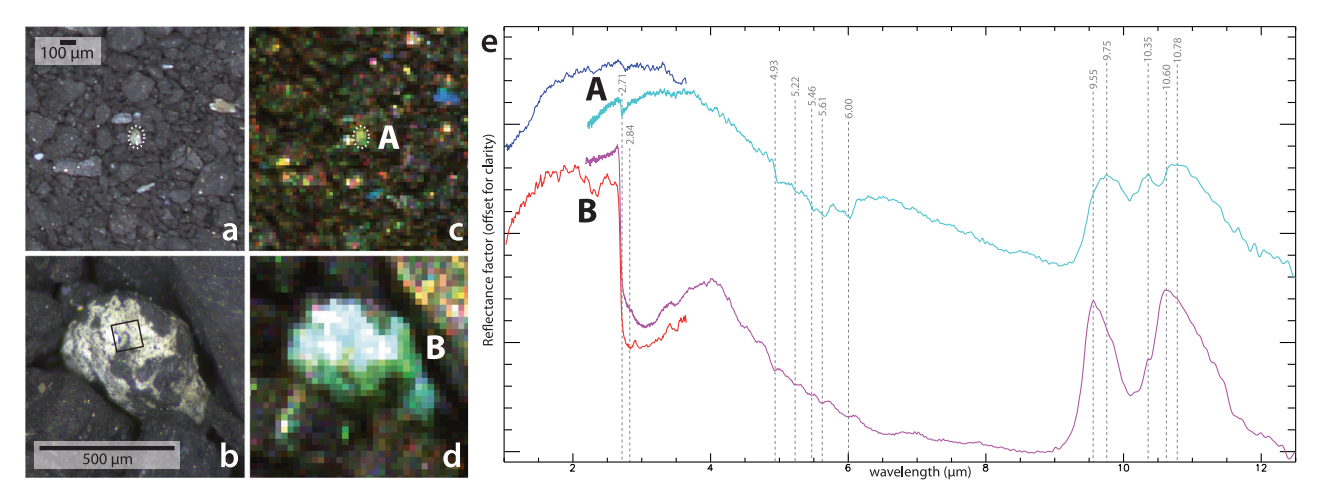


Fig. 6 | Examples of type 4 spectra observed by MicrOmega within Bennu samples. a, b Visible images show the context where the grains/inclusions are detected. In MicrOmega RGB composite image of the same areas ( $\mathbf{c}$ ,  $\mathbf{d}$ ), they are highlighted by a dashed circle (R: 3.34  $\mu$ m, G: 2.50  $\mu$ m, B: 1.20  $\mu$ m). e Corresponding MicrOmega average spectra (15 pixels for spectrum A in blue and 135 pixels for spectrum B in red) and complementary mid-IR spectra obtained with a  $\mu$ -FT-IR

spectrometer (spot size of  $50\,\mu m$  spot for spectrum A in cyan and  $100\,\mu m$  for spectrum B in purple). The footprint of the mid-IR observation for Region B is indicated by a black square in the visible image. These combined near-IR-mid-IR analyses did not require any extraction from the facility, preventing any exposure of the sample to the terrestrial environment.

on Ryugu samples in terms of peak position (within the uncertainties) suggesting similarities in the overall composition of the phyllosilicates, in particular regarding their Mg/Fe content<sup>12</sup>. Bennu and Ryugu samples also display similarly a weak feature at  $-3.4\,\mu\text{m}$ , indicative of the presence of aliphatic CH in organics and of carbonates. This feature is slightly more pronounced in Bennu samples than in Ryugu samples (-3–4% for Bennu samples vs. -2% for Ryugu sample, Fig. 1). Its interpretation in terms of enhanced abundance of a given constituent (organics or carbonates) must be consistent with both elemental abundances of carbon slightly higher in Bennu than in Ryugu samples

(4.7 % in Bennu vs. 3.8 % in Ryugu  $^{3,14}$  ,) and a higher H/C atomic ratio in Ryugu samples  $^{14,43}$  .

Other similarities are also seen for a variety of OH-, H<sub>2</sub>O-, NH- (a fraction of which are in the form of NH<sub>4</sub><sup>+</sup>)-rich components, as well as carbonates, which can be observed at sub-millimetre scale. Both the HAMPs and the other NH-bearing phases show strong spectral similarities with those observed in Ryugu samples<sup>4,15,44</sup>. Carbonates also appear to be dominated at MicrOmega scale by (Mg,Ca) and (Mg,Fe) types, as in Ryugu samples<sup>11</sup>. Altogether, the spectral similarities between alteration products such as carbonates, HAMPs and the

dominating Mg-rich phyllosilicates, as well as the NH-rich components in both Ryugu and Bennu samples suggest resembling, though not necessarily identical, initial material, environmental conditions and formation processes. In particular, the detection of  $\rm NH_4^+$  as part of HAMP-rich compounds indicates that the parent body of Bennu formed or accreted a part of its material in the outer Solar System, in agreement with  $^{43}$ . The preservation of HAMPs both in Bennu and Ryugu samples also indicates that their further evolution has remained at low temperature (<-70 °C if the struvite is considered as analog  $^{45}$ ), in agreement with  $^{17}$  that derived a temperature range of 20–55 °C based on the salt formation sequence, and similar to what has been proposed for Ryugu (e.g.,  $^8$ ).

Some significant differences could nonetheless be observed between Bennu and Ryugu samples. The large amounts of samples analyzed in this study, combined with the extensive set of similarities identified between two distinct objects reduce the likelihood that these differences translate possible biases from the collection process. The band depth of the ~2.7 µm feature that dominates down to the millimetre scale is weaker in Bennu samples compared to Ryugu samples (10–12 % vs. 12–18% in Ryugu bulk samples<sup>4</sup>). The grain size does not seem to be the cause of this discrepancy as the Bennu bulk samples show variations of similar magnitude, whether measured in areas dominated by larger (mm-size) grains or by finer fractions (Supplementary Fig. 2). Both the Ryugu and Bennu samples exhibit a similar band shape (Fig. 1), which would argue for a similar mineralogical composition. The lower ~2.7 µm band depth could then be due to 1) a less extended aqueous alteration of the initial anhydrous precursor (i.e., less crystallized Mg-rich phyllosilicates, e.g., 46), 2) a more space weathered material<sup>12</sup>, or 3) the presence of more opaque material that could lower (or even hide) the signature. No systematic band shift, which would indicate a stronger contribution from space weathered material (e.g., 47), is observed on average relative to Ryugu samples. The reflectance level, acquired in identical observational conditions, is also similar between Ryugu and Bennu samples (Fig. 1). The first hypothesis is, thus, favored over the two others, Additionally, a greater amount of anhydrous silicates has been observed in Bennu samples (~2 vol%³) compared to Ryugu samples (<0.5 vol%⁴8,). Here we also show that large olivine grains (larger than a few tens of microns), either intact or slightly altered, are present in Bennu samples. Such grains/inclusions have not, so far, been identified in the Ryugu bulk samples in similar observations by MicrOmega4. We cannot rule out that this constitutes one of the potential minor biases induced by the collection process of Hayabusa2. The differences could also translate a possible exogenous origin of these compounds, as exogenic bright boulders with spectral properties similar to ordinary chondrites meteorites have been observed at the surface of Bennu<sup>49</sup>. The preservation of a greater abundance of precursor material could be consistent with the less extended aqueous alteration discussed above. In addition, the detection, here, of volatile-rich species in Bennu samples indicates that the temperature remained low throughout their history and therefore that these olivine grains/inclusions do not originate from thermal metamorphism but are remnants from the initial material present on the parent body.

The close proximity in most spectral properties at both centimetre and sub-mm scales between Bennu and Ryugu samples, thus, suggests that they experienced broadly similar formation and evolutionary processes. Differences would thus originate from a greater diversity of local environments - possibly at very fine/sub-mm spatial scale - on their primary parent body. Another possibility would be that Bennu sampled a greater variety of areas and, thus, of environments during the disruption and reaccretion of its parent body.

One of the most critical findings in the samples returned from Ryugu was the presence of Hydrated Ammonium-Magnesium-Phosphorus-rich (HAMP) grains<sup>15</sup>. Such compounds were identified through the analysis of pristine Ryugu samples by the MicrOmega

instrument, followed by the extraction and further ex-situ characterization of a few of these grains by complementary methods (SEM/EDS, DRX, mid-IR spectroscopy<sup>15</sup>,). These compounds most likely overlap with the Mg-phosphates observed by refs. 6,8. Similarly<sup>3</sup>, and then<sup>17</sup> reported the detection of Mg-phosphates in Bennu samples. Here we show that at least a fraction of them are actually HAMP-rich compounds, very similar in their IR signature to those observed in Ryugu samples. This last point is critical: as IR spectroscopy is sensitive to vibration modes, it implies a similar molecular structure between HAMP-rich compounds from Ryugu and Bennu.

Reference <sup>15</sup> proposed a formation scenario for the HAMPs found in Ryugu that is mainly based on thermodynamics and where the availability of NH<sub>4</sub><sup>+</sup> and the formation of carbonates and phosphates are interconnected. It can be roughly summarized as follows: the early formation of Ca-rich carbonates depletes the environment in Ca, which then favors the formation of HAMPs with regards to Ca-rich phosphates (apatites). Indeed, the latter is much more stable and would, thus, have formed preferentially if Ca was available. The observation of similar main families of carbonates in Ryugu and Bennu samples suggests a common process on the parent bodies to form HAMP-rich compounds. The colocalization of Mg-phosphates with Ca-rich carbonates observed by<sup>17</sup> and the formation sequence that they proposed tend to confirm the formation scenario developed by<sup>15</sup>.

HAMPs, therefore, appear as a generic product of the process that drove the early evolution of a given class of primitive parent bodies. Such a result then supports the high relevance of these salt-type compounds in delivering phosphorous and nitrogenous species, with organics from the matrix, to the primitive Earth which could efficiently contribute to the organic chemistry towards life, as proposed by<sup>15</sup>.

Another critical outcome concerns the near-IR spectral slope observed on Bennu samples. While Ryugu was categorized as a type Cb asteroid in the  $^{50}$  taxonomy classification (based on the 0.45-2.45  $\mu m$ spectral range)<sup>51</sup>, Bennu was categorized as a type B<sup>52-54</sup>. Both types belong to the C-complex category, the main difference concerning the spectral slope; red (positive) for Ryugu and blue (negative) for Bennu. The blue slope of the Bennu spectrum was confirmed by the remote sensing observations after the arrival at Bennu by the OSIRIS-REx mission<sup>55</sup>. Our results show strong similarities between Ryugu and Bennu average NIR spectral properties on the returned bulk samples. and in particular the observation of a red slope for both Ryugu and Bennu samples. A difference in the NIR spectral slope between lab and remote sensing observations could be due to physical properties of the surface of the asteroid (e.g., texture, grain size, porosity, e.g., 56-59) and/ or space weathering (e.g., 47,60). Both Bennu and Ryugu's surfaces are mainly covered by highly porous boulders<sup>51,61,62</sup>. However, contrary to Ryugu, Bennu's surface appears to be dominated by two major populations of boulders with different radiative, thermo-physical and density properties<sup>63-65</sup>. Such differences at metre-scale could also lead to differences in the production of fines<sup>66</sup>, possibly sparsely present at the surface (e.g., 62). Additionally 67, has shown that the freshest crater on Ryugu and Bennu exhibited similar spectral behavior in the visible and that space weathering would then affect their spectra in opposite directions (bluing for Bennu and reddening for Ryugu). While we cannot rule out that the small differences in the mineralogical composition highlighted by our analyses, could cause these different trends on the spectral slope (e.g., 47), we would favor a driving role of macroscopic physical parameters (e.g., texture) coupled to space weathering. Such a result would advocate for a re-evaluation of the significance of the near-IR spectral slope when assessing the compositional properties of the different asteroid populations.

The characterization of both Bennu and Ryugu bulk samples, using identical techniques, reveals that they share most near-IR spectral properties, implying similar initial material and evolution processes, yet not strictly identical. In particular some significant differences related to the depth of the ~2.7 µm feature and the

occurrence of olivine at MicrOmega scale could be observed between Bennu and Ryugu samples. These most likely reflect some small scale heterogeneities in the level of aqueous processes on the parent body. The strong similarity, however, that we show here in the detected compounds, indicates that the main characteristics of Ryugu and Bennu samples emerge as a general property of an entire class of objects formed in the outer part of the protoplanetary disk. Subsets of these objects would have been possibly later injected in the inner Solar System, delivering compounds of high biochemical relevance such as HAMPs<sup>15</sup> and organic compounds<sup>9,14,43</sup> to the terrestrial planets.

#### Methods

#### Samples

In August 2024, JAXA/ESCuC received 0.5 wt.% of unprocessed and unbiased samples returned by OSIRIS-REx<sup>20</sup>. The samples consist of five different aggregate samples, including numerous particles larger than 1 mm: OREX-800058-0, OREX-800111-0, OREX-800116-0, OREX-800120-0 and OREX-800125-0 on the OSIRIS-REx Samples Database from NASA, renamed ORX-19000, ORX-29000, ORX-39000, ORX-49000 and ORX-59000 by JAXA. All samples were extracted from trays than contained materials directly collected from inside of the TAGSAM head cover: ORX-19000 from material collected underneath the mylar flap and ORX-29000, ORX-39000, ORX-49000 and ORX-59000 from material collected after the TAGSAM container was fully disassembled. The selection process is fully described in<sup>20</sup>. The weights for the individual bulk samples are as follows: 0.183 g for ORX-19000, 0.135 g for ORX-29000, 0.152 g for ORX-39000, 0.047 g for ORX-49000 and 0.148 g for ORX-59000<sup>20</sup>.

Similarly to the Ryugu samples, the Bennu samples are maintained pristine in a dedicated curation facility at ESCuC<sup>20</sup>. The first campaign of analyses, performed in September 2024, was dedicated to the characterization of the five "bulk samples".

#### MicrOmega analyses

The MicrOmega instrument is a near-IR hyperspectral microscope originally developed for the ExoMars 2028 rover mission<sup>21</sup> and that is capable to characterize in a non-destructive and non-invasive manner the mineralogical and molecular composition of samples down to the scale of ~20 µm. The model installed at the ESCuC of JAXA (Sagamihara, Japan) is a copy of the ExoMars model. The instrument works as follows: MicrOmega sequentially illuminates the sample at different wavelengths with an incidence angle of ~35°; for each illuminated wavelength, a 256 × 250 pixels image is acquired in a 'nadir' configuration (pixel size of 22.5  $\mu$ m). A hyperspectral  $(x, y, \lambda)$  cube is built by scanning the different monochromatic channels in the 0.99-3.65 µm wavelength range. Thanks to the use of an acousto-optic tunable filter (AOTF) as dispersive system, with a full width at half maximum of ~20 cm<sup>-1</sup>, the wavelengths can be selected and repeated in any order with minimum sampling steps of ~2 cm<sup>-1</sup>. For the baselined operations, the typical number of spectral channels per cube varies between ~200 and ~300.

MicrOmega is mounted on a copper plate maintained at  $10\,^{\circ}\text{C}$  in an ultraclean- $N_2$  purged chamber. For the analysis, the samples are introduced within a sample chamber part of the main curation facility suite, separated from the MicrOmega chamber by a near-IR-transparent sapphire ( $Al_2O_3$ ) window, and continually flowed with  $N_2$ . This setup is similar to the one used in the Hayabusa2 curation facility for the analysis of the Ryugu samples.

Each of the five bulk samples was deposited on a dedicated sapphire sample holder (15 mm diameter at the base of the sample cavity, 23 mm diameter at the top) set on a polished gold-coated mirror, similarly to what was done for Ryugu samples<sup>4</sup>. The sample holder was set on a  $(x,y,z,\theta,\Delta)$  moving stage (3 axes translation, 360° rotation in the horizontal plane,  $\pm 10^\circ$  tilt), remotely controlled, enabling to position the entire surface of the sample within the MicrOmega Field of

View (useful area of  $\sim$ 5 × 5 mm<sup>2</sup>) and to illuminate the grains with different geometries.

Each bulk sample was fully covered by a mosaic of 10-15 MicrOmega acquisitions, some with a different focus to account for irregularities of the top surface of the grains. Such analyses were repeated for a couple of different orientations (e.g.,  $\theta$  = 0°, 90°,180°, 270°) to minimize the effects of shadowing. Additional acquisitions were also performed on specific regions of interest.

The wavelength calibration of the illumination beam has been performed at the Institut d'Astrophysique Spatiale using two reference targets: a Wavelength Calibration Standard from Labsphere and a calcite pellet. Radiometric calibration was performed first at the Institut d'Astrophysique Spatiale and then periodically within the Curation Facility, using two reference targets: Spectralon 99% and Infragold from Labsphere. The potential contribution of the sapphire window to the signal has been removed using acquisitions performed without any sample in the field of view. The radiometric calibration is evaluated to be better than 20% in absolute value and -1% in relative value (from one spectral channel to the next). The spectral accuracy is evaluated to be better than 5 nm. Details about the calibration procedure and performances can be found in refs. 68 and <sup>12</sup>.

## Complementary characterizations by visible microscopy and mid-IR spectrometry

For each bulk sample, complementary optical images were obtained with a Leica visible microscope, set next to the MicrOmega instrument. Importantly, the MicrOmega data were also used to identify and locate regions of interest, that were then targeted by a  $\mu\text{-FT-IR}$  spectrometer JASCO IRT-5200/VIR-200 with a 2.0–13  $\mu\text{m}$  spectral range (footprint of -50–100  $\mu\text{m}$ ), providing access to complementary spectral signatures, while still within the Curation facility. The spectral resolution is 4 cm $^{-1}$  and the spectral sampling is 1 cm $^{-1}$ . The microscope's incidence, emission, and phase angles are 0°, 0°, and 0°, respectively. Calibration was performed using a gold mirror, as well as an Infragold reference target from Labsphere.

#### Data availability

Spectral data and images are provided in the Source Data files. IR spectral data obtained at ESCuC will also be available in the catalogue of Bennu samples (https://www.darts.isas.jaxa.jp/curation/hayabusa2/). Other data and images on the Bennu samples are available at the same address. Source data are provided with this paper.

#### References

- Morbidelli, A. et al. Source regions and time scales for the delivery of water to Earth. Meteorit. Planet. Sci. 35, 1309–1320 (2000).
- Yada, T. et al. Preliminary analysis of the Hayabusa2 samples returned from C-type asteroid Ryugu. Nat. Astron. 6, 214–220 (2022).
- Lauretta, D. S. et al. Asteroid (101955) Bennu in the laboratory: Properties of the sample collected by OSIRIS-REx. Meteorit. Planet. Sci. 59, 2453–2486 (2024).
- Pilorget, C. et al. First compositional analysis of Ryugu samples by the MicrOmega hyperspectral microscope. *Nat. Astron.* 6, 221–225 (2022).
- Ito, M. et al. A pristine record of outer Solar System materials from asteroid Ryugu's return sample. Nat. Astron. 6, 1163–1171 (2022).
- Nakamura, E. et al. On the origin and evolution of the asteroid Ryugu: A comprehensive geochemical perspective. *Proc. Jpn. Acad. Ser. B* 98, 227–282 (2022).
- Yokoyama, T. et al. Samples returned from the asteroid Ryugu are similar to Ivuna-type carbonaceous meteorites. Science 379, 6634 (2023). article id. abn7850.

- Nakamura, T. et al. Formation and evolution of carbonaceous asteroid Ryugu: Direct evidence from returned samples. Science 379, 6634 (2023), article id. abn8671.
- Yabuta, H. et al. Macromolecular organic matter in samples of the asteroid (162173). Ryugu. Sci. 379, 634 (2023). article id. abn9057.
- Paquet, M. et al. Contribution of Ryugu-like material to Earth's volatile inventory by Cu and Zn isotopic analysis. *Nat. Astron.* 7, 182–189 (2023).
- Loizeau, D. et al. Constraints on Solar System early evolution by MicrOmega analysis of Ryugu carbonates. *Nat. Astron.* 7, 391–397 (2023).
- Le Pivert-Jolivet, T. et al. Space weathering and pristineness of Ryugu samples from MicrOmega spectral analyses. *Nat. Astron.* 7, 1445–1453 (2023).
- Brunetto, R. et al. Ryugu's anhydrous ingredients and their spectral link to primitive dust from the outer solar system. *Astrophys. J. Lett.* 951, 8 (2023).
- Naraoka, H. et al. Soluble organic molecules in samples of the carbonaceous asteroid (162173). Ryugu. Sci. 379, 6634 (2023).
- Pilorget, C. et al. Phosphorus-rich grains in Ryugu samples with major biochemical potential. Nat. Astron. 8, 1529–1535 (2024).
- Imae, N. et al. Mineralogical approach on laboratory weathering of uncontaminated Ryugu particles: Comparison with Orgueil and perspective for storage and analysis. *Meteorit. Planet. Sci.* 59, 1705–1722 (2024).
- McCoy, T. J. et al. An evaporite sequence from ancient brine recorded in Bennu samples. *Nature* ume 637, 1072–1077 (2025).
- Le Pivert-Jolivet, T. et al. Water in Ryugu as a property of processes in its parent body. Astronomy & Astrophysics, Volume 695, id.A168, 10 pp. (2025)
- Connolly, H. C. et al. An overview of the petrography and petrology of particles from aggregate samples from asteroid Bennu, Meteoritics and Planetary Science 1-18 (2025)
- Astromaterials Science Research Group, Institut d'Astrophysique Spatiale, Université Paris-Saclay, CNES, S. Nakahara, et al. (2025) OSIRIS-REx Bennu Sample Curatorial Dataset. https://doi.org/10. 17597/ISAS.DARTS/CUR-Bennu-description.
- Bibring, J.-P. et al. The MicrOmega Investigation Onboard ExoMars. Astrobiology 17, 621–626 (2017).
- Furukawa, S. et al. Near-infrared spectral variation in Ryugu particles and Implication for rapid space weathering by solar UV radiation. Sci. Rep. 15, 14613 (2025).
- 23. Gaffey, S. J. Spectral reflectance of carbonate minerals in the visible and near infrared (0.35–2.55 um): anhydrous carbonate minerals. *J. Geophys. Res.* **92**, 1429–1440 (1987).
- Bishop, J. L. et al. Spectral properties of anhydrous carbonates and nitrates. Earth Space Sci. 8, e2021EA001844 (2021).
- Mahlke, M. et al. Aqueous alteration of Ryugu's parent body: Insights from carbonates seen by MicrOmega. Europlanet Science Congress 2024, held 8-13 September, 2024 at Freie Universität, Berlin, Germany. id. EPSC2024-174. https://doi.org/10.5194/epsc2024-174 (2024).
- Eisenberg, D. and Kauzmann, W. The structure and properties of water, New-York: Oxford University Press, 296 pp. (1969)
- Bishop, J. L. et al. Infrared spectroscopic analyses on the nature of water in montmorillonite. Clays Clay Min. 42, 702–716 (1994).
- 28. Libnau, F. O. et al. Spectra of water in the near- and mid-infrared region. *Vibrational Spectrosc.* **7**, 243–254 (1994).
- 29. Banks, E. et al. Chemistry of Struvite Analogs of the Type MgMPO4-6H2O (M+ = K+ Rb+ Cs+, T1+, NH4+). Inorg. Chem. 14,(1975)
- Berg, B. et al. Reflectance spectroscopy (0.35-8 μm) of ammoniumbearing minerals and qualitative comparison to Ceres-like asteroids. *Icarus* 265, 218–237 (2016).

- Reddy, B. J. et al. A Near Infrared spectroscopic study of the phosphate mineral pyromorphite Pb5(PO4)3Cl. Spectrochimica Acta Part A: Mol. Biomolecular Spectrosc. 71, 430–435 (2008).
- 32. Jastrzebski, W. et al. Infrared spectroscopy of different phosphates structures. Spectrochim. Acta A 79, 722–727 (2011).
- Takir, D. et al. Nature and degree of aqueous alteration in CM and CI carbonaceous chondrites. *Meteorit. Planet. Sci.* 48, 1618–1637 (2013). Nr.
- Clark, R. N. et al. High spectral resolution reflectance spectroscopy of minerals. J. Geophys. Res. 95, 12653–12680 (1990).
- Bowey and Hofmeister. Overtones of silicate and aluminate minerals and the 5-8 μm ice bands of deeply embedded objects. Monthly Not. R. Astronomical Soc. 358, 1383–1393 (2005).
- Yan, W. et al. Effect of second Si-O vibrational overtones/combinations on quantifying water in silicate and silica minerals using infrared spectroscopy, and an experimental method for its removal. *Phys. Chem. Miner.* 49, 5 (2022).
- 37. Salisbury, J. W. et al. Infrared (2.1–25 mm) Spectra of Minerals. The Johns Hopkins University Press, Baltimore and London (1991)
- 38. Clark, R. N. et al. USGS digital spectral library splib06a. US Geological Survey, Digital Data Series 231, http://speclab.cr.usgs.gov/spectral.lib06 (2007).
- 39. Hamilton, V. E. Thermal infrared (vibrational) spectroscopy of Mg–Fe olivines: A review and applications to determining the composition of planetary surfaces. *Chem. der Erde* **70**, 7–33 (2010).
- 40. Miller, G. H. et al. The natural occurrence of hydroxide in olivine. *Phys. Chem. Miner.* **14**, 461–472 (1987).
- Lemaire, C. et al. The effect of silica activity on the incorporation mechanisms of water in synthetic forsterite: a polarised infrared spectroscopic study. Contrib. Miner. Pet. 147, 48–57 (2004).
- Farmer, V. C. The Infrared Spectra of Minerals. Mineralogical Society, London (1974).
- Glavin, D. P. et al. Abundant ammonia and nitrogen-rich soluble organic matter in samples from asteroid (101955) Bennu. *Nat. Astron.* 9. 199–210 (2025).
- 44. Jiang, T. et al. Detection of NH-rich compounds in Bennu pristine samples via IR characterization at JAXA Curation Center and comparison with Ryugu, EGU General Assembly 2025, Vienna, Austria, 27 Apr-2 May 2025, EGU25-16881. https://doi.org/10.5194/egusphere-egu25-16881 2025.
- Feng, T. et al. Evolution of ephemeral phosphate minerals on planetary environments. ACS Earth Space Chem. 5, 1647–1656 (2021).
- Aléon-Toppani, A. et al. Correlated IR-SEM-TEM studies of three different grains from Ryugu: From the initial material to post-accretional processes. Geochim. et. Cosmochim. Acta 371, 1–30 (2024).
- Lantz, C. et al. Ion irradiation of carbonaceous chondrites: A new view of space weathering on primitive asteroids. *Icarus* 285, 43–57 (2017).
- 48. Yamaguchi, A. et al. Insight into multi-step geological evolution of C type asteroids from Ryugu particles. *Nat. Astron.* **7**, 398–405 (2023).
- 49. Le Corre, L. et al. Characterization of Exogenic Boulders on the Near-Earth Asteroid (101955) Bennu from OSIRIS-REx Color Images. *Planet. Sci. J.* **2**, 114 (2021).
- 50. DeMeo, F. E. et al. An extension of the Bus asteroid taxonomy into the near-infrared. *Icarus* **202**, 160–180 (2009).
- Sugita, S. et al. The geomorphology, color, and thermal properties of Ryugu: Implications for parent-body processes. Science 364, 6437 (2019).
- Clark, B. E. et al. Asteroid (101955) 1999 RQ36: Spectroscopy from 0.4 to4 µm and meteorite analogs. *Icarus* 216, 462–475 (2011).
- Binzel, R. P. et al. Compositional distributions and evolutionary processes for the near-Earth object population: Results from the MIT-Hawaii Near-Earth Object Spectroscopic Survey (MITHNEOS). *Icarus* 324, 41–76 (2019).

- 54. Mahlke, M. et al. Asteroid taxonomy from cluster analysis of spectrometry and albedo. *Astron. Astrophys.* **665**, 32 (2022).
- Hamilton, V. et al. Evidence for widespread hydrated minerals on asteroid (101955) Bennu. Nat. Astron. 3, 332–340 (2019).
- Johnson, T. V. & Fanale, F. P. Optical properties of carbonaceous chondrites and their relationship to asteroids. J. Geophys. Res. 78, 8507–8518 (1973).
- 57. Cloutis, E. A. et al. Spectral reflectance properties of carbonaceous chondrites: 1. CI chondrites. *Icarus* **212**, 180–209 (2011a).
- Cloutis, E. A. et al. Spectral reflectance properties of carbonaceous chondrites: 2. CM chondrites. *Icarus* 216, 309–346 (2011b).
- Kiddell, C. B. et al. Spectral reflectance of powder coatings on carbonaceous chondrite slabs: Implications for asteroid regolith observations. J. Geophys. Res.: Planets 123, 2803–2840 (2018).
- Lantz, C. et al. Space weathering trends on carbonaceous asteroids:
  A possible explanation for Bennu's blue slope?. *Icarus* 302, 10–17 (2018).
- Okada, T. et al. Highly porous nature of a primitive asteroid revealed by thermal imaging. *Nature* 579, 518–522 (2020).
- 62. DellaGiustina, D. N. et al. Properties of rubble-pile asteroid (101955) Bennu from OSIRIS-REx imaging and thermal analysis. *Nat. Astron.* **3**, 341–351 (2019).
- DellaGiustina, D. N. et al. Variations in color and reflectance on the surface of asteroid (101955) Bennu. Science 370, 6517 (2020).
- 64. Rozitis, B. et al. Asteroid (101955) Bennu's weak boulders and thermally anomalous equator. Sci. Adv. 6, eabc3699 (2020).
- Rozitis, B. et al. High-Resolution Thermophysical Analysis of the OSIRIS-REx Sample Site and Three Other Regions of Interest on Bennu. J. Geophys. Res.: Planets 127, e2021JE007153 (2022).
- 66. Cambioni, S. et al. Fine-regolith production on asteroids controlled by rock porosity. *Nature* 598 (2021)
- 67. Yumoto, K. et al. Comparison of optical spectra between asteroids Ryugu and Bennu: II. High-precision analysis for space weathering trends. *Icarus* **420**, 116204 (2024).
- Riu, L. et al. Calibration and performances of the MicrOmega instrument for the characterization of asteroid Ryugu returned samples. Rev. Sci. Instrum. 93, 054503 (2022).

#### **Acknowledgements**

We deeply thank the Hayabusa2 team for the opportunity to be part of this outstanding project. We are grateful to the NASA Headquarters and Johnson Space Center curation team for providing the Bennu samples to the Extraterrestrial Sample Curation Center (ESCuC) of JAXA. We also thank the Centre National d'Etudes Spatiales (CNES) for its full support. LN acknowledges the support as part of France 2030 program ANR-11-IDEX-0003, attributed through the Astrophysical Axis of the Graduate School of Physics of the University Paris-Saclay. RS was supported by the European Commission through a Marie Skłodowska-Curie Postdoctoral Fellowship (Grant Agreement No. 101110008).

#### **Author contributions**

T.O., K.H., R.F., M.N., T.Y., K.Y., C.P., J.-P.B. and V.H. conceived and designed the experiments and the workflow. T.O., K.H., R.F., M.A., Y.E., S.K., A.Mi, M.N., R.T., T.U., T.Y and K.Y. led the curation activities of the OSIRIS-REx samples. K.H., D.L., L.N., L.R., R.S., C.L., M.M., Y.E., S.K., A.Mi., F.P., R.T., K.Y., C.P., J.-P.B. and V.H. performed the measurements. D.L., T.J., L.N., R.S., K.H., M.M., L.R., R.B., D.B., A.A., V.H., C.L., F.P., C.P. and J.-P.B. contributed to the data processing, analysis and interpretation. C.P., T.O., J.-P.B., D.L., K.H., L.N., L.R., R.S., T.J., M.M., R.B., D.B., R.F., M.A., A.A., Y.E., V.H., S.K., C.L., A.Mi., A.M., M.N., F.P., R.T., T.U., T.Y., K.Y. were involved in the discussions of the results and the preparation of the manuscript.

#### **Competing interests**

The authors declare no competing interests.

#### **Additional information**

**Supplementary information** The online version contains supplementary material available at https://doi.org/10.1038/s41467-025-65438-z.

**Correspondence** and requests for materials should be addressed to C. Pilorget.

**Peer review information** *Nature Communications* thanks Van T.H. Phan and the other, anonymous, reviewer(s) for their contribution to the peer review of this work. A peer review file is available.

**Reprints and permissions information** is available at http://www.nature.com/reprints

**Publisher's note** Springer Nature remains neutral with regard to jurisdictional claims in published maps and institutional affiliations.

Open Access This article is licensed under a Creative Commons Attribution-NonCommercial-NoDerivatives 4.0 International License, which permits any non-commercial use, sharing, distribution and reproduction in any medium or format, as long as you give appropriate credit to the original author(s) and the source, provide a link to the Creative Commons licence, and indicate if you modified the licensed material. You do not have permission under this licence to share adapted material derived from this article or parts of it. The images or other third party material in this article are included in the article's Creative Commons licence, unless indicated otherwise in a credit line to the material. If material is not included in the article's Creative Commons licence and your intended use is not permitted by statutory regulation or exceeds the permitted use, you will need to obtain permission directly from the copyright holder. To view a copy of this licence, visit <a href="https://creativecommons.org/licenses/by-nc-nd/4.0/">https://creativecommons.org/licenses/by-nc-nd/4.0/</a>.

© The Author(s) 2025